

## 2-Bit Quad Band Reconfigurable Intelligent Surface for Modern Wireless Communications

Vimal Kumar<sup>#</sup>, Amit Sikder<sup>#</sup>, Gunjan Srivastava<sup>§</sup> and Akhilesh Mohan<sup>\*,\*</sup>

<sup>#</sup>Department of Electronics and Communication Engineering, IIT Roorkee, Roorkee - 247 667, India

<sup>§</sup>Department of Electronics and Communication Engineering, Graphic Era (Deemed to be) University, Dehradun- 248002, India

<sup>\*</sup>E-mail: am@ece.iitr.ac.in

### ABSTRACT

This paper presents a 2-bit Reconfigurable Intelligent Surface (RIS) fed by an Antipodal Vivaldi Antenna (AVA) to achieve broader angular coverage and avoid feed blockage in four distinct frequency bands. The RIS consists of a 20×20 array of unit cells, each containing varactor diodes to control the reflection phase in the four operational bands. The feed antenna is placed at an equivalent focal point of the RIS to illuminate it. The feed antenna has a peak gain of 10.4 dBi at 8.4 GHz and a -10 dB impedance bandwidth of over 10 GHz. The peak gains (sidelobe levels) of the proposed RIS at 3.5 GHz, 4.5 GHz, 5.7 GHz, and 8.4 GHz are 14.6 dBi (-29 dB), 11.2 dBi (-13 dB), 16.4 dBi (-26 dB), and 17.2 dBi (-23.7 dB), respectively. Also, at 3.5 GHz, 4.5 GHz, 5.7 GHz, and 8.4 GHz, the beam steering range (scan loss) offered by the RIS are 28° (3.9 dB), 23° (2.4 dB), 70° (3 dB), and 76° (5 dB), respectively. Overall, the RIS multiband functionality expands its potential application areas.

**Keywords:** Antipodal Vivaldi Antenna (AVA); Beam steering; Polarization insensitive; Reconfigurable intelligent surface (RIS)

### NOMENCLATURE

$\epsilon_r$	: Dielectric constant
$\tan \delta$	: Loss tangent
$q$	: Feed function constant
$F$	: Focal length
$D$	: Diameter (length/width) of the RIS

### 1. INTRODUCTION

Overcoming electromagnetic (EM) propagation obstacles and covering a wider area is becoming more challenging in fifth-generation (5G) and beyond telecommunications as the urban area and industry expand rapidly. Current approaches, such as using massive Multiple Input Multiple Output (MIMO) systems or deploying additional base stations (BSs) to extend radio coverage, help to minimize interference, boost power gain, and improve spectrum efficiency by transmitting highly focused signals with significant gain to each user. However, implementing these systems is more expensive and complex<sup>1,2</sup>.

Reconfigurable Intelligent Surfaces (RISs) offer an efficient and cost-effective way to minimize blockage effects and enhance network coverage in 5G and beyond networks without significantly compromising signal quality. An RIS is a flat two-dimensional surface with reconfigurable unit cells that can individually adjust the phase of reflected or transmitted signals. This capability allows the RIS to steer incoming waves in specific directions.

Reconfigurability is achieved through active components such as liquid crystals, PIN diodes, and varactor diodes, which

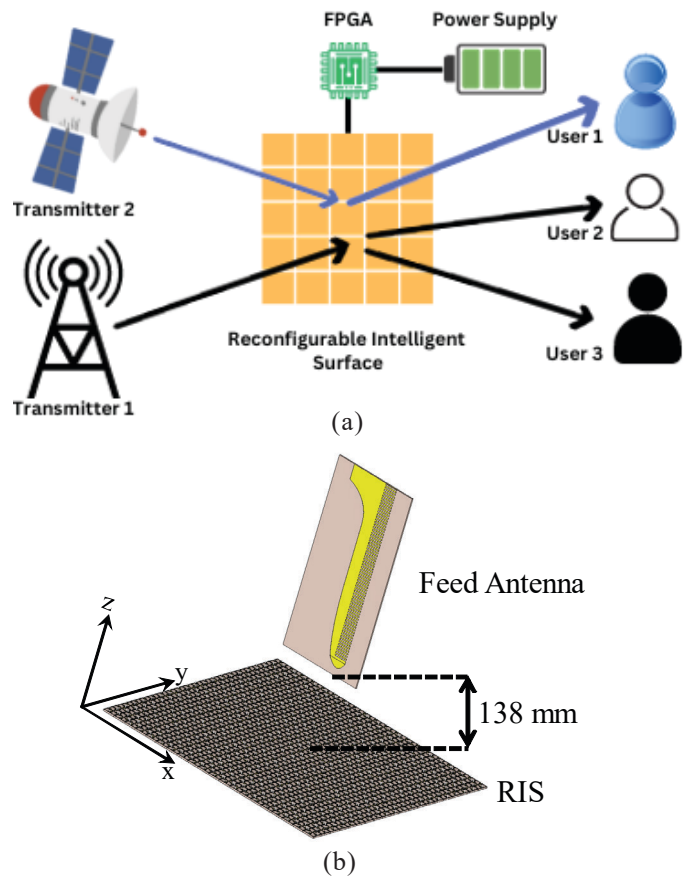


Figure 1. (a) Beam-steering and signal directional control using RIS; and (b) the RIS configuration.

can be controlled and programmed using embedded devices like Arduino, FPGA, and Raspberry Pi. Non-line-of-sight (NLoS) propagation allows the RIS to redirect incoming EM waves toward a receiver through dynamical reflection. RIS designs also incorporate low-loss substrates to minimize dielectric loss<sup>3-4</sup>. A conceptual representation of the RIS working mechanism is shown in Fig. 1(a).

Several ways to design RIS are presented in the open literature<sup>5-10</sup>. Cao, X.<sup>5</sup>, *et al.* demonstrate a time-modulated reflectarray illuminated by an antipodal fermi antenna has been used for RIS applications. It can provide multifunctionality, including reflection, beam scanning, and beam shaping under different application scenarios. The unit cell of the time-modulated reflectarray consists of a PIN diode connected to a phase delay line. With the ON and OFF condition of the PIN diode, 180° of reflection phase difference has been obtained at 10 GHz. Since the unit cells are quantized in only 2-state (1-bit), the quantization loss is as high as 2.56 dB<sup>6</sup>. Moreover, it operates in a single band with an element bandwidth of less than 13 %. Wu, L.<sup>7</sup>, *et al.* present an amplifying RIS, a combination of the power amplifier and RIS, has been reported. It consists of an aperture-coupled patch-type unit cell excited with a power amplifier-loaded microstrip delay line. The active mode gain is close to 10 dB with a fractional bandwidth of

nearly 18.2 %. However, it works in only one band and shows a slightly high cross-polarization level due to the presence of a power amplifier. Some of the available literature manipulates Liquid Crystal's molecule to engineer the relative permittivity of the unit cell for desired phase change<sup>8-10</sup>.

This paper presents a 2-bit RIS with 20×20 varactor diode-based unit cells for quad-band applications. The RIS offers a broader and more affordable application range due to its multiband functionality. A comb-shaped periodic slit edge antipodal Vivaldi antenna (AVA) is used as the feed antenna. As shown in Fig. 1(b), the AVA is positioned in front of the RIS at the optimal focal length to analyze the characteristics of the reflected wave. The RIS can enhance antenna gain by up to 8 dB and effectively redirect incoming waves to 76°.

## 2. ANTENNA CONFIGURATION

The proposed RIS features a periodic arrangement of 20×20 unit cells, which are illuminated by an AVA. Each unit cell is designed with a multilayer structure comprising a ground plane on one side of the substrate and a radiating patch on the other, loaded with four U-shaped stubs encased by a square ring. The square ring further incorporates four inward-facing I-shaped stubs that converge toward the center of the U-stub. Two of the U-shaped stubs are integrated with varactor diodes, enabling dynamic phase tuning. Biasing for the varactor diodes is achieved through strategically placed vias connecting the center of the patch and specific points on the square ring to the ground plane, as shown in Fig. 2(a)-(c). By varying the capacitance of the varactor diodes, the unit cell can achieve a phase profile modulation of 2-bit across four distinct frequency bands. This configuration enables precise control over the reflected wavefront, facilitating multifunctional performance across multiple operating frequencies. The proposed antenna system can be a good candidate for a multiband beam-steering antenna system and as an RIS.

## 3. METHODOLOGY

### 3.1 2-bit Unit Cell Design

The unit cell consists of one dielectric and two metallic layers. The top layer has a square metal loop with four microstrip lines pointing toward the center, and a square metal with four U-shaped metal structures, two diodes are used to connect them, as shown in Fig. 2(a). In Fig. 2(b), the bottom layer is a metallic sheet acting as a ground plane. Two metallic vias are inserted from the top to the bottom metal layer, as illustrated in Fig. 2(c), to bias the diodes. The copper is used as metal with a thickness of 0.035 mm, while the substrate is Rogers RT/Duroid 5880 with a thickness of 1.57 mm, a relative dielectric constant ( $\epsilon_r$ ) of 2.2 and a loss tangent ( $\tan\delta$ ) of 0.0009. Varactor diode BB837 is selected for its high capacitance and low series resistance. This unit cell is simulated in CST Microwave Studio with appropriate boundary conditions and Floquet port excitation. The simulation result shows that the unit cell can efficiently modify the phase from 0° to 270° with a 90° interval in four different frequency bands: 3.23 to 3.74 GHz (band-1), 5 to 5.16 GHz (band-2), 5.75 to 5.94 GHz (band-3), and 8.4 GHz (band-4) by adjusting the diode capacitance as shown in Fig. 2 (d). The capacitance values and the unit cell's ideal

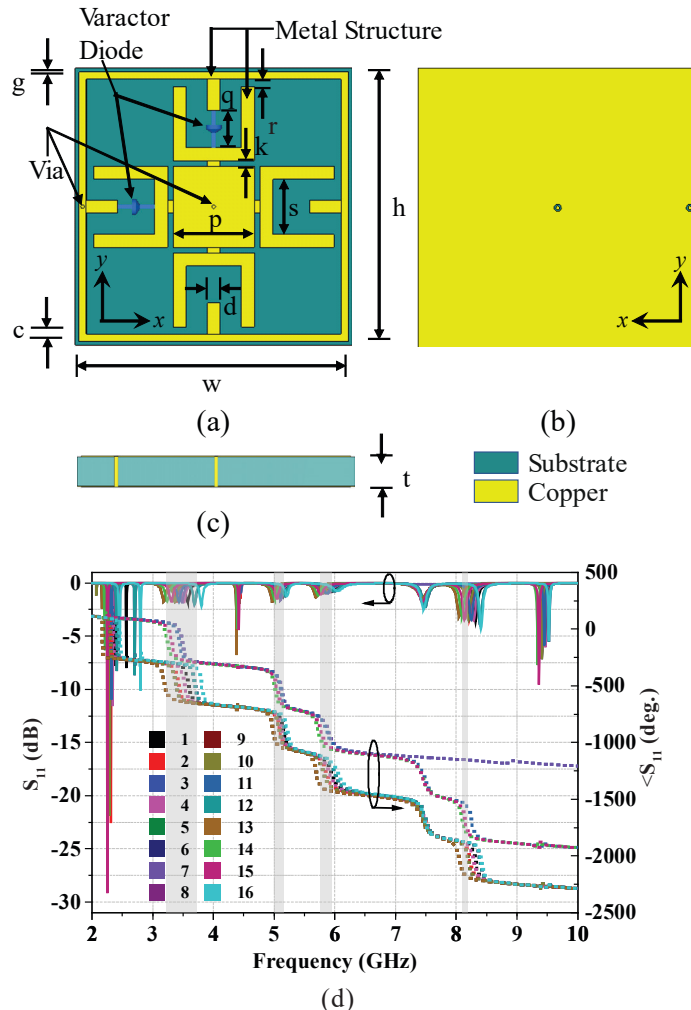


Figure 2. (a) Top view; (b) Bottom view; (c) Side view of the unit cell; and (d) S-parameters of the unit cell.

Table 1. Sixteen capacitance values for quad-band

Band-1	Coding State	#1	#2	#3	#4
	Capacitance (pF)	0.62	0.95	0.78	0.71
Band-2	Coding State	#5	#6	#7	#8
	Capacitance (pF)	6.11	1.07	0.78	0.51
Band-3	Coding State	#9	#10	#11	#12
	Capacitance (pF)	6.11	1.08	0.9	0.51
Band-4	Coding State	#13	#14	#15	#16
	Capacitance (pF)	6.11	2.55	1.41	0.45

Table 2. Geometric parameters of the unit cells

c	d	g	h	k	p
0.4	0.7	0.2	14.6	0.5	4
q	r	s	t	w	
2	0.4	3	1.65	14.6	

All dimensions are in mm.

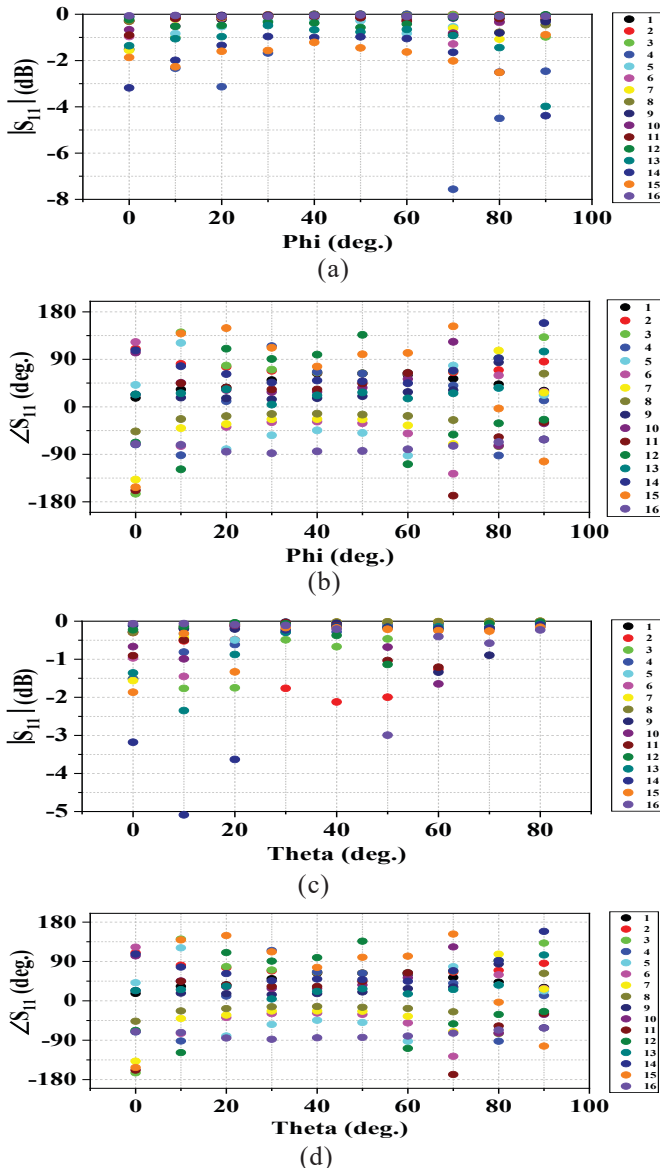


Figure 3. (a) Reflection coefficient; (b) reflection phase for different polarization angles; (c) Reflection coefficient; and (d) reflection phase for different incident angles.

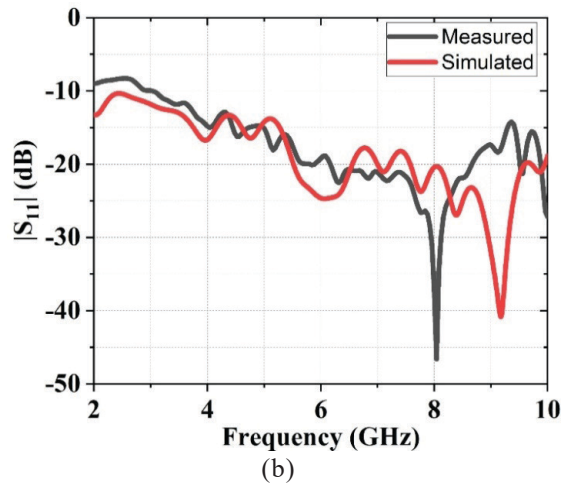
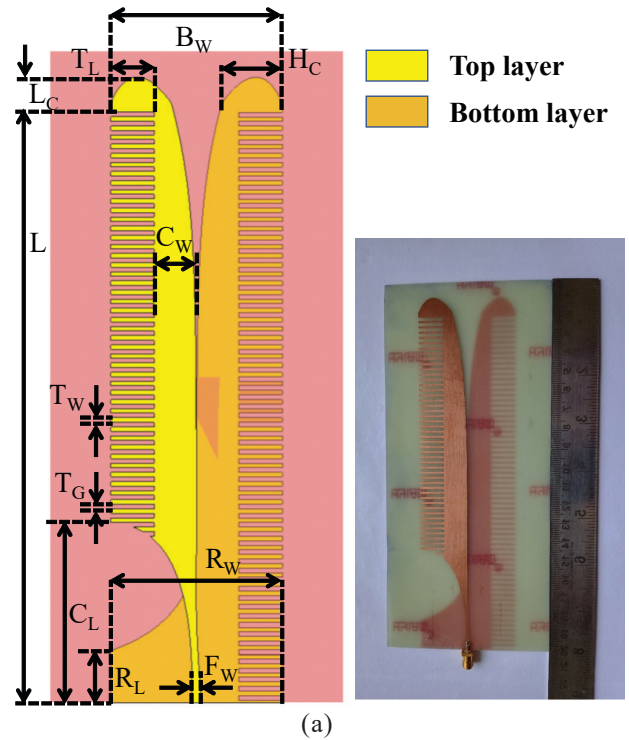


Figure 4. (a) Simulated design and fabricated prototype; and (b) Simulated and measured S-parameters of the AVA.

geometrical characteristics are detailed in Tables 1 and 2<sup>11</sup>. in four different frequency bands: 3.23 to 3.74 GHz (band-1), 5 to 5.16 GHz (band-2), 5.75 to 5.94 GHz (band-3), and 8.4 GHz (band-4) by adjusting the diode capacitance as shown in Fig. 2 (d). The capacitance values and the unit cell’s ideal geometrical characteristics are detailed in Tables 1 and 2<sup>11</sup>.

The incident angle and polarization angle stability of the unit cell is further investigated to validate its effectiveness in a large array. Fig. 3(a) presents the polarization sensitivity in terms of absorption loss across a range of angles from 0° to 90°, simulated at 10° intervals. The results demonstrate that loss remains within 3 dB for angles up to 70°, with some values exceeding this threshold at larger angles. In contrast, Fig. 3(b) illustrates the polarization sensitivity with respect to phase variation, showing a reduction in the phase interval at 20°, reaching its minimum at 40°. Similarly, Fig. 3(c) examines angular stability by depicting absorption loss across incident

**Table 3. Geometric parameters of the AVA**

$F_w$	$R_L$	$R_w$	$C_L$	$T_g$	$T_w$
2.87	15.9	52.7	55.3	1.45	1.35
$L$	$T_L$	$B_w$	$H_c$	$L_c$	
184.1	13.35	52.7	18.57	7.9	

All dimensions are in mm.

angles ranging from  $0^\circ$  to  $80^\circ$ , simulated at  $10^\circ$  increments. The results indicate that absorption losses for all coding states generally remain within the 3 dB threshold up to  $80^\circ$ . However, as shown in Fig. 3(d), the phase interval decreases significantly, reaching  $20^\circ$ .

### 3.2 Feed Antenna Design

Horn antennas are commonly used to feed an RIS. However, the horn antenna can cause significant feed blockage at lower frequencies. To address this issue and avoid feed blockage, in this paper, an AVA has been used<sup>12</sup>. The feed antenna has three layers, with a dielectric layer between the top and bottom metal layers. In this configuration, the dielectric substrate adopted is FR-4, with a thickness of 1.57 mm. Both metal layers feature symmetrical designs, including a periodic slit edge and an exponential radiator in the form of a comb. Additionally, a rectangular metal plane is integrated into the bottom layer to serve as a ground, while the top metal layer is designed to facilitate a  $50 \Omega$  port impedance, as shown in Fig. 4 (a). The AVA has been in-house fabricated by PCB technology with the optimum dimensions listed in Table 3. The S-parameter of the fabricated AVA is then measured using a VAN. The simulated and measured S-parameters are shown in Fig. 4(b).

In the simulated scenario, the proposed feed antenna exhibits an impedance bandwidth of  $|S_{11}| \leq -10$  dB, from 2 GHz

to 10 GHz. However, in the physical prototype, the impedance bandwidth,  $|S_{11}| \leq -10$  dB, starts at 3 GHz and extends beyond 10 GHz. Although discrepancies exist between the simulated and measured values, the operational frequencies remain within the feed antenna bandwidth, thus confirming that the RIS remains unaffected. Furthermore, the radiation pattern of the feed antenna is mapped with a single variable function to calculate optimum aperture efficiency and feed position. A single-variable feed function,  $\cos^q(\theta)$ , correlates with the AVA radiation pattern. At frequencies of 3.5, 4.5, 5.7, and 8.4 GHz, the gain ( $q$  value) is approximately 9.3 dBi ( $\approx 8$ ), 8.09 dBi ( $\approx 4$ ), 8.36 dBi ( $\approx 4$ ), and 10.4 dBi ( $\approx 12$ ), respectively.

### 3.3 RIS Structure and Simulation Setup

To achieve optimal aperture efficiency and prevent slipover and illumination losses, the focal length to diameter ratio ( $F/D$ ) is set at 0.75. The RIS comprises  $20 \times 20$  unit cells. As depicted in Fig. 5, the phase difference equation<sup>13</sup> is used to calculate the desired reflection phase ( $\angle S_{11}$ ) for different beam orientations. The phase center of each band is situated in the far field of the AVA due to the RIS being positioned 138 mm from the feed antenna.

As illustrated in Fig. 1(b), the antenna is arranged to transmit the incident wave polarized along the y-axis. CST Microwave Studio is utilized to perform the full-wave EM simulation to validate this RIS.

## 4. RESULTS AND DISCUSSION

A focused beam is constructed using the proposed RIS, and the primary beam's direction can be altered by adjusting the capacitance values of the unit cells, as depicted in Fig. 5. The simulated peak gain at 3.5 GHz is 14.6 dBi when the main beam is at  $0^\circ$ . It diminishes as the beam deviates to  $28^\circ$ , resulting in a scan loss of 3.9 dB, as illustrated in Fig. 6(a).

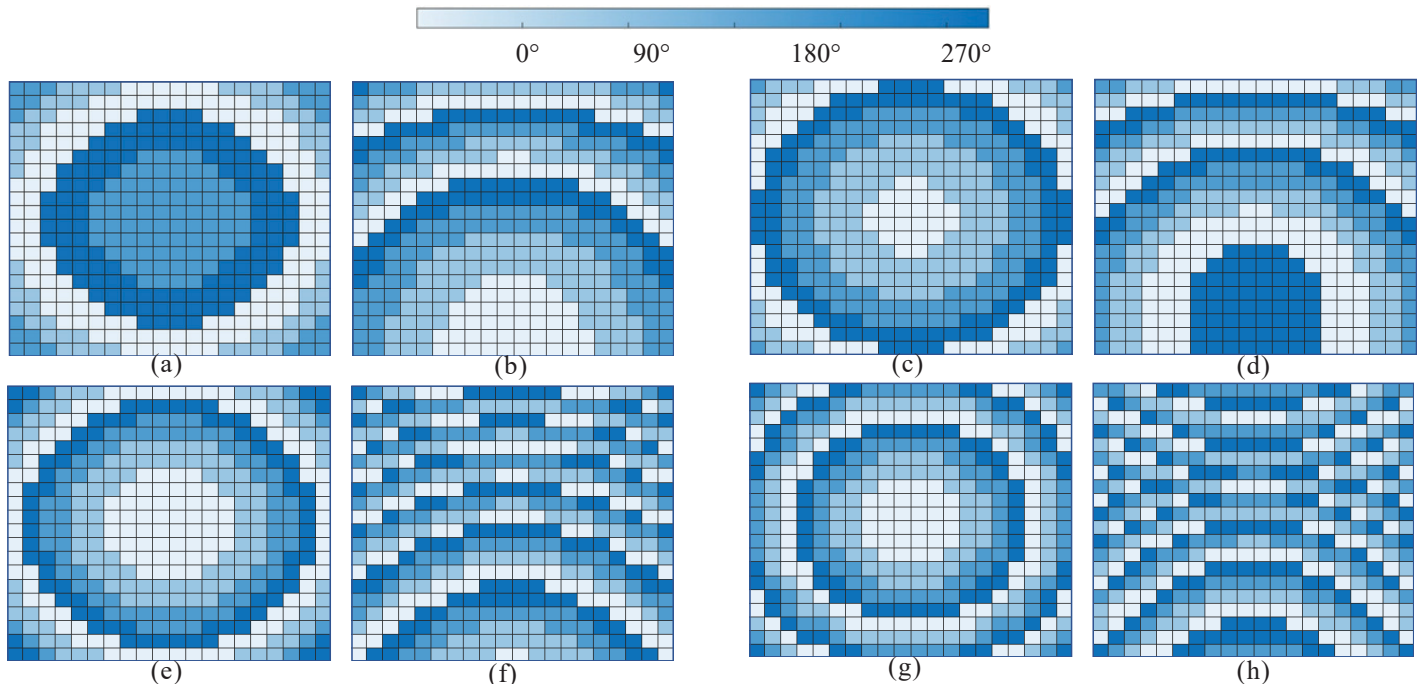


Figure 5. Unit cell phase distribution at 3.5 GHz (a) for  $\theta = 0^\circ$ ; (b)  $\theta = 40^\circ$ , at 4.5 GHz; (c) for  $\theta = 0^\circ$ ; (d)  $\theta = 30^\circ$ , at 5.7 GHz; (e) for  $\theta = 0^\circ$ ; (f)  $\theta = 80^\circ$ , and 8.4 GHz; and (g) for  $\theta = 0^\circ$ , (h)  $\theta = 80^\circ$ .

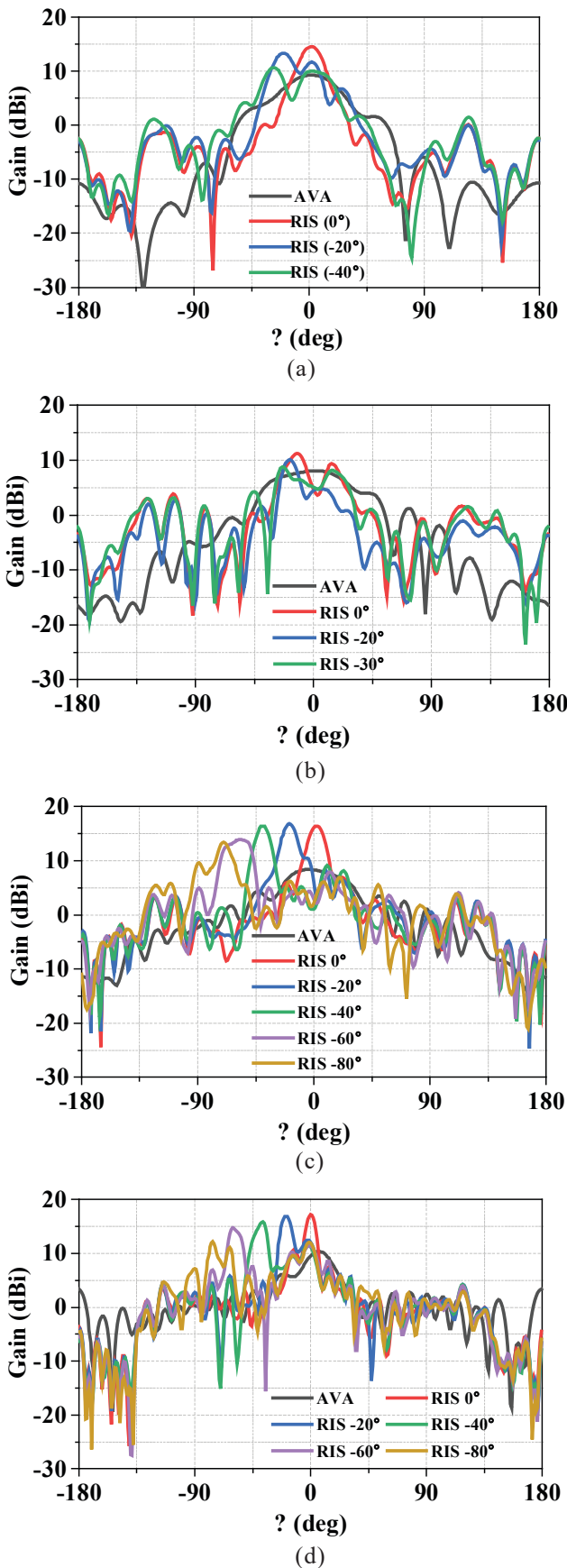


Figure 6. Feed antenna radiation pattern and beam scanning result of the proposed RIS at (a) 3.5 GHz; (b) 4.5; (c) 5.7 GHz; and (d) 8.4 GHz.

The simulated sidelobe level consistently remains below -11.3 dB for any beam angle. Similarly, at  $\theta = 0^\circ$ , the simulated peak gain at 4.5 GHz is 11.2 dBi and progressively decreases as the beam shifts to  $23^\circ$ . Due to the low scanning range compared to band-1, The scan loss diminishes from 3.9 dB to 2.4 dB. The simulated sidelobe level remains consistently below -9.5 dB for every beam angle, as depicted in Fig. 6 (b). Proceeding to the 5.7 GHz band, the simulated peak gain at  $\theta = 0^\circ$  is 16.4 dBi, decreasing to 12.4 dBi at a  $70^\circ$  beam shift. The scan loss for beam steering in this band amounts to 4 dB. The simulated sidelobe level is less than -17.2 dB at all beam angles, as shown in Fig 6(c). Lastly, in the 8.4 GHz band, the simulated peak gain at  $\theta = 0^\circ$  is 17.2 dBi. However, it decreases to 12.2 dBi when the beam is adjusted to  $76^\circ$ . The beam steering scan loss has reached 5 dB due to the band's higher coverage area, leading to higher signal loss. The simulated sidelobe level remains consistently below -13.3 dB at all beam angles, as presented in Fig. 6(d).

### 5. CONCLUSIONS

To reduce feed obstruction for lower frequency bands, this work presents the design and simulation of a single-layer multiband reconfigurable intelligent surface (RIS) excited by an Antipodal Vivaldi Antenna (AVA). The AVA has a 10.4 dBi peak gain and a side lobe level of -14.7 dB, offering a wide bandwidth to minimize feed obstruction. At 3.5 GHz, 4.5 GHz, 5.7 GHz, and 8.4 GHz, the proposed RIS enhances the gains by approximately 5 dBi, 3 dBi, 8 dBi, and 7 dBi, respectively. Additionally, it demonstrates beam scanning capability up to  $76^\circ$ . The proposed antenna can be employed in modern applications beyond 5G communications.

### REFERENCES

1. Chang, C.Y. & Chou, H.T. A millimeter-wave binary reconfigurable intelligent surface on a low-cost FR4 substrate. *In* 18<sup>th</sup> European Conference on Antennas and Propagation (EuCAP), Glasgow, United Kingdom, 2024, pp. 1-4. doi: 10.23919/EuCAP60739.2024.10501260.
2. Fonseca, F.H.S.; Morais, G.I.; Clemente, G.C. & Pagan, C.J.B. Tunable 2-bit unit cell based in a square loop for reconfigurable intelligent surface application. *In* 2022 Asia-Pacific Microwave Conference (APMC), Yokohama, Japan, 2022, pp. 875-877. doi: 10.23919/APMC55665.2022.9999789.
3. Joy, A.T.; Tishchenko, A.; Taghvaei, H.; Botham, P.; Burton F. & Khalily, M. From reconfigurable intelligent surfaces to holographic MIMO surfaces and back. *In* 18<sup>th</sup> European Conference on Antennas and Propagation (EuCAP), Glasgow, United Kingdom, 2024, pp. 1-5. doi: 10.23919/EuCAP60739.2024.10501134.
4. Wang, R.; Yang, Y.; Makki, B. & Shamim, A. A wideband reconfigurable intelligent surface for 5G millimeter-wave applications. *IEEE Transact. Antennas and Propag.*, 2024, **72**(3), 2399-2410. doi: 10.1109/TAP.2024.3352828.
5. Cao, X.; Chen, Q.; Tanaka, T.; Kozai, M. & Minami, H. A 1-bit time-modulated reflect array for reconfigurable-

- intelligent-surface applications. *IEEE Transact. Antennas and Propag.*, 2023, **71**(3), 2396-2408.  
doi: 10.1109/TAP.2022.3233659.
6. Yang, H.; Yang, F.; Xu, S.; Li, M.; Cao, X. & Gao, J. A study of phase quantization effects for reconfigurable reflectarray antennas. *IEEE Antennas Wireless Propag. Lett.*, 2017, **16**, 302-305.  
doi: 10.1109/LAWP.2016.2574118.
  7. Wu, L.; Lou, K.; Ke, J.; Liang, J.; Luo, Z.; Dai, J. Y.; Cheng, Q. & Cui, T. J. A wideband amplifying reconfigurable intelligent surface. *IEEE Transact. Antennas and Propag.*, 2022, **70**(11), 10623-10631.  
doi: 10.1109/TAP.2022.3187137.
  8. Youn, Y.; An, D.; Kim, D.; Hwang, M.; Choi, H.; Kang, B. & Hong, W. Liquid-crystal-driven reconfigurable intelligent surface with cognitive sensors for self-sustainable operation. *IEEE Transact. Antennas and Propag.*, 2023, **71**(12), 9415-9423, 2023.  
doi: 10.1109/TAP.2023.3312814.
  9. Li, X.; Sato, H.; Fujikake, H. & Chen, Q. Development of two-dimensional steerable reflectarray with liquid crystal for reconfigurable intelligent surface applications. *IEEE Transact. Antennas and Propag.*, 2024, **72**(3), 2108-2123.  
doi: 10.1109/TAP.2024.3354054.
  10. Kim, H.; Oh, S.; Bang, S.; Yang, H.; Kim, B. & Oh, J. Independently polarization manipulable liquid- crystal-based reflective metasurface for 5g reflectarray and reconfigurable intelligent surface. *IEEE Transact. Antennas and Propag.*, 2023, **71**(8), 6606-6616.  
doi: 10.1109/TAP.2023.3283136.
  11. Sikder, A.; Kumar, V.; Srivastava, G. & Mohan, A. A 2-bit tunable unit cell for quad-band reconfigurable intelligent surface. *In Second International Conference on Microwave, Antenna and Communication (MAC)*, Visakhapatnam, India, 2024, pp. 1-4.  
doi: 10.1109/WAMS59642.2024.10528150.
  12. Sun, M.; Qing, X. & Chen, Z.N. 60-GHz antipodal Fermi antenna on PCB. *In Proceedings of the 5<sup>th</sup> European Conference on Antennas and Propagation (EUCAP)*, Rome, Italy, 2011, pp. 3109-3112.
  13. Kumar, V.; Mohan, A. & Ghosh, B. Beam-steering transmitarray antenna for 5G application. *IEEE Wireless Antenna and Microwave Symposium (WAMS)*, Ahmedabad, India, 2023, pp. 1-4.  
doi: 10.1109/WAMS57261.2023.10242958.

## CONTRIBUTORS

**Mr Vimal Kumar** obtained his M.Tech degree from the Department of Avionics, Indian Institute of Space Science and Technology Thiruvananthapuram, India. Currently, he is pursuing a Ph.D. from the Department of Electronics and Communication Engineering, IIT Roorkee, India. His research interests are space-fed high-gain antennas, MIMO antennas, and passive microwave circuits. In the current study he contributed in terms of conceptualisation, simulation, and manuscript writing.

**Mr Amit Sikder** obtained his MTech degree from the Department of Electronics and Communication Engineering from IIT Roorkee, India. His research interests are high-gain antennas, MIMO antennas, and passive microwave circuits. In the current study he contributed in terms of simulation, fabrication, and measurements.

**Dr Gunjan Srivastava** obtained her PhD degree from the IIT, Dhanbad, India in Microwave Engineering and working as an Associate Professor in the Department of Electronics and Communication Engineering at Graphic Era (Deemed to be) University, Dehradun. Her research interests are design of ultra-wideband, reconfigurable, differential, SIW, MIMO, and self-multiplexing antennas. In the current study she contributed in terms of simulation and manuscript writing.

**Dr Akhilesh Mohan** obtained PhD degree in Microwave Engineering from IIT, Kanpur, Uttar Pradesh, India and working as a Faculty Member at the Department of Electronics and Communication Engineering, IIT, Roorkee, Uttarakhand, India. His research interests include: Design of microwave filters, antennas, and absorbers for wireless communication systems. In the current study he has contributed as conceptualisation and manuscript-editing.